Check for updates

DOI: 10.1002/cssc.200900243

Renewable H_2 from Glycerol Steam Reforming: Effect of La_2O_3 and CeO_2 Addition to Pt/Al_2O_3 catalysts.

Tiziano Montini,[a] Rakesh Singh,[b, c] Piyali Das,[b, d] Barbara Lorenzut,[a] Nicolás Bertero,[b, e] Pietro Riello,[f] Alvise Benedetti,[f] Giuliano Giambastiani,[g] Claudio Bianchini,[g] Sergey Zinoviev,[b] Stanislav Miertus,[b] and Paolo Fornasiero*[a, b]

Glycerol is the main byproduct of biodiesel production and its increased production volume derives from the increasing demand for biofuels. The conversion of glycerol to hydrogen-rich mixtures presents an attractive route towards sustainable biodiesel production. Here we explored the use of Pt/Al_2O_3-based catalysts for the catalytic steam reforming of glycerol, evidencing the influence of La_2O_3 and CeO_2 doping on the catalyst activity and selectivity. The addition of the latter metal oxides to a Pt/Al_2O_3 catalyst is found to significantly improve the glycerol steam reforming, with high H_2 and CO_2 selectivities. A good catalytic stability is achieved for the $Pt/La_2O_3/Al_2O_3$ system working at 350 °C, while the $Pt/CeO_2/Al_2O_3$ catalyst sharply deactivates after 20 h under similar conditions. Studies carried out on fresh and exhausted catalysts reveal that both systems maintain high surface areas and high Pt dispersions. Therefore, the observed catalyst deactivation can be attributed to coke deposition on the active sites throughout the catalytic process and only marginally to Pt nanoparticle sintering. This work suggests that an appropriate support composition is mandatory for preparing high-performance Pt-based catalysts for the sustainable conversion of glycerol into syngas.

Introduction

The use of renewables, such as biomass, is essential for a sustainable development of our society. The conversion of renewable resources into either clean fuels or chemicals is attracting growing interest because of the continuous reduction of fossil hydrocarbon supplies.[1] Depending on the starting biomass-based material fuel production is either sustainable, or not. First-generation biofuels essentially comprise ethanol and biodiesel, obtained from sugar fermentation and transesterification of animal fats or vegetable oils, respectively. Unfortunately, the long-term production of these biofuels is not sustainable because it can seriously compromise both food supplies and biodiversity. The use of biomasses that consist of the residual nonfood parts of current crops represents a challenging goal for the production of second-generation biofuels, starting from the extraction of complex molecules (lignin or cellulose) from woods or fibrous biomasses. To this purpose, several catalytic processes for the production of useful chemicals and feedstocks via hydrolysis of lignocellulose residues have been already investigated.[2] Finally, third-generation biofuels can be produced from marine biomasses, such as algae, with higher energy balances than those obtained from land crops.

Hydrogen plays an important role in this context. In fact, hydrogen is not only a fundamental chemical for important industrial processes but it is also considered an attractive and clean energy vector for fuel-cell technology.[1] Nowadays, hydrogen is mostly used for the purification of fuel by removing sulfur and nitrogen (HDS and HDN processes), ammonia synthesis, cracking/refining processes, methanol production, hydrogenation reactions, and fuel production via Fisher–Tropsch synthesis.[3] In the energy field, hydrogen is more properly conceived as an energy vector rather than an energy source because its production requires energy from other sources.[4,5] Because the current industrial production of hydrogen is essen-

[a] Dr. T. Montini, Dr. B. Lorenzut, Prof. P. Fornasiero
Department of Chemical Sciences, ICCOM-CNR Research Unit
University of Trieste
via L. Giorgieri 1, 34127 Trieste (Italy)
Fax: (+39) 040 5583903
E-mail: pfornasiero@units.it

[b] Dr. R. Singh, Dr. P. Das, Dr. N. Bertero, Dr. S. Zinoviev, Dr. S. Miertus, Prof. P. Fornasiero
International Centre for Science and High Technology (ICS-UNIDO)
AREA Science Park, Padriciano 99, 34012 Trieste (Italy)

[c] Dr. R. Singh
Polymer Science and Engineering Division
National Chemical Laboratory
Homi Bhabha Road, Pune 411008 (India)

[d] Dr. P. Das
Energy Environment Technology Development (EETD) Division
The Energy and Resources Institute (TERI)
Darbari Seth Block, India Habitat Centre, Lodhi Road, New Delhi-110003 (India)

[e] Dr. N. Bertero
Catalysis Science and Engineering Research Group (GICIC)
Instituto de Investigaciones en Catálisis y Petroquímica (INCAPE)
FIQ-UNL-CONICET, Santiago del Estero 2654, Santa Fe 3000 (Argentina)

[f] Prof. P. Riello, Prof. A. Benedetti
Department of Physical Chemistry
Ca' Foscari University of Venice
Via Torino 155, 30170 Venice (Italy)

[g] Dr. G. Giambastiani, Dr. C. Bianchini
Institute of Chemistry of OrganoMetallic Compounds, ICCOM-CNR
Via Madonna del Piano 10
50019 Sesto Fiorentino (Italy)

Supporting Information for this article is available on the WWW under http://dx.doi.org/10.1002/cssc.200900243.

 © 2010 Wiley-VCH Verlag GmbH & Co. KGaA, Weinheim WILEY InterScience DISCOVER SOMETHING GREAT

tially based on fossil fuels (ca. 90% from methane and ca. 5% from other hydrocarbons), during the last few years extensive research efforts have been devoted to developing new processes for its clean production.[6–14]

The implementation of new biorefineries for the valorization of biomasses, especially those obtained from agricultural residues, is considered a successful alternative for the preparation of chemicals (including H_2) and biofuels.[15–17] Several methods have been proposed for the H_2 production from renewables: biomass reforming and water electrolysis using solar, wind, or hydroelectric power.[18] Recently biodiesel has become one of the most promising biofuels,[19–22] although its relatively high production costs are a limitation to its worldwide acceptance. The recovery of byproducts (mainly glycerol) from biodiesel production and their use as new feedstocks in biorefineries[23,24] can strongly contribute to bringing down the overall production costs of biodiesel.

Among these byproducts, glycerol represents a valuable hydrogen source.[4,5] Recent review articles account for a large variety of catalytic and enzymatic transformations of glycerol into high-value chemical derivatives.[2,25–30] The use of this feedstock to obtain hydrogen has gained a lot of attention due to the increasing hydrogen demand, mainly for fuel-cell applications.[31]

Glycerol can be converted into syngas by steam reforming (SR) according to the following reaction:

$$C_3H_8O_3 + 3\,H_2O \rightarrow 3\,CO_2 + 7\,H_2 \quad (1)$$

This process can be formally written as a combination of two separate reactions: glycerol decomposition into H_2 and CO [Equation (2)] followed by the water-gas shift (WGS) equilibrium [Equation (3)]:

$$C_3H_8O_3 \rightarrow 3\,CO + 4\,H_2 \quad (2)$$

$$CO + H_2O \rightleftharpoons CO_2 + H_2 \quad (3)$$

Typically, glycerol SR is a catalytic process that occurs in the vapor phase at atmospheric pressure and temperatures of up to 900 °C. Because of its endothermic nature, high temperatures, low pressures, and a high steam-to-glycerol ratio are generally required to obtain high substrate conversions.[4] When compared with the aqueous phase reforming (APR) protocol, SR requires more energy to vaporize the biomass solutions. Despite this general disadvantage, SR may be preferred to the APR protocol because of the lower amounts of contaminating side-products produced. Indeed, under SR conditions, the amount of methane and higher hydrocarbons can be significantly reduced with respect to the APR conditions,[11,32] just by running the reaction at atmospheric pressure instead of higher pressures (as required by the APR process).[31] In addition, the APR process still needs to be optimized for concentrated solutions.[11,33]

Many metal catalysts have been investigated for glycerol SR, among which Ru,[34–36] Rh,[35,37] Ir,[35,38,39] Pd,[35,40,41] Pt,[35,37,42–45] Co,[38] and mainly Ni[35,38,41,44,46–50] catalysts are the most representative ones. Pt is a good candidate for glycerol SR, allowing for efficient C–C, O–H, and C–H bond cleavages with high activities and selectivities. By contrast, other metals require some promoters to ensure similar performances.[40,49,51] A wide range of supports for the active metal sites in the glycerol SR reaction has also been tested, varying from acidic[35] to basic,[47] in many cases without paying attention to the non-innocent role of these materials in the catalytic process. An efficient catalyst for H_2 production from glycerol is expected to break-up the substrate through C–C, O–H, and C–H bond cleavages, at the same time promoting the elimination of metal-passivating carbon monoxide via the WGS reaction. Finally, such a catalyst should not promote either C–O cleavage or CO or CO_2 hydrogenation to form alkanes and more polar compounds, respectively.[52]

Many research efforts are required to scale up the glycerol SR reaction from the laboratory to an industrial scale. Indeed, some important properties of the catalytic system, such as stability and selectivity towards H_2 production, must be carefully considered before taking this step. Moreover, catalyst deactivation resulting from coke deposition on the catalyst surface is one of the most important limitations to industrial glycerol SR. It is well-known that CeO_2 can act as a non-innocent support, preventing, to some extent, coke deposition at the active sites of the catalyst.[38,53,54] Furthermore, CeO_2 can efficiently catalyze the WGS reaction,[38,55–57] favoring CO elimination and preventing the catalyst from passivation/deactivation.

Acidic catalyst supports, such as Al_2O_3, can promote side reactions during the SR process, leading to saturated[20] or unsaturated hydrocarbons.[58] One possible alternative to control the acidic site density of these supports is their impregnation with basic oxides such as La_2O_3 or CeO_2. In this Full Paper we report on the preparation of Al_2O_3/CeO_2- and Al_2O_3/La_2O_3-supported Pt nanoparticles, and on their use as efficient catalytic systems for H_2 production via glycerol SR. We demonstrate that the acidity of the support is reduced by means of basic additives, such as CeO_2 and La_2O_3, thereby improving the catalyst stability and selectivity and reducing, at the same time, the formation of undesirable products and coke deposition. A complete characterization of the new catalytic systems is provided, with the aim of rationalizing the fundamental role of the support composition on the catalytic performance of the Pt nanoparticles.

Results and Discussion

Catalytic activity

Initial experiments under SR conditions showed a strong influence of the composition of the catalyst support on the conversion of glycerol into syngas. Figure 1 shows the conversion of glycerol into gaseous products, calculated based on their flow rates at the outlet of the reactor (after condensation of the nonvolatile compounds), as a function of the catalyst temperature, while Figure 2 shows the composition of the gas phase produced throughout the catalytic process, as obtained by GC analysis.

A typical Pt/Al_2O_3 catalyst exhibited a poor activity towards glycerol SR at low temperatures, with a minimum in the glycer-

 © 2010 Wiley-VCH Verlag GmbH & Co. KGaA, Weinheim

1864564x, 2010, 5, Downloaded from https://chemistry-europe.onlinelibrary.wiley.com/doi/10.1002/cssc.200900243 by CONICET Consejo Nacional de Investigaciones, Wiley Online Library on [07/12/2023]. See the Terms and Conditions (https://onlinelibrary.wiley.com/terms-and-conditions) on Wiley Online Library for rules of use; OA articles are governed by the applicable Creative Commons License

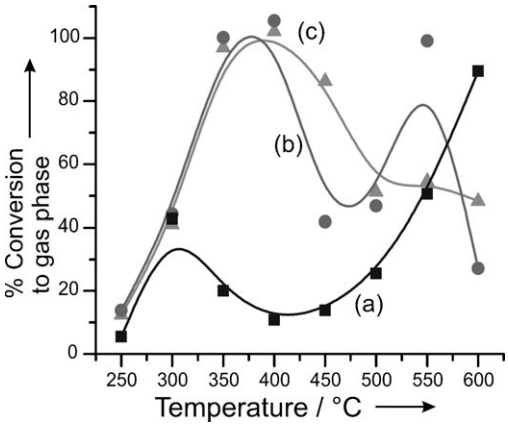

Figure 1. Glycerol conversion to gas-phase products as a function of catalyst temperature on (a) Pt/Al_2O_3, (b) $Pt/La_2O_3/Al_2O_3$, and (c) $Pt/CeO_2/Al_2O_3$. Conditions: 1.00 g catalyst, 0.32 mL min^{-1} $C_3H_8O_3$ (30 wt%; aqueous solution).

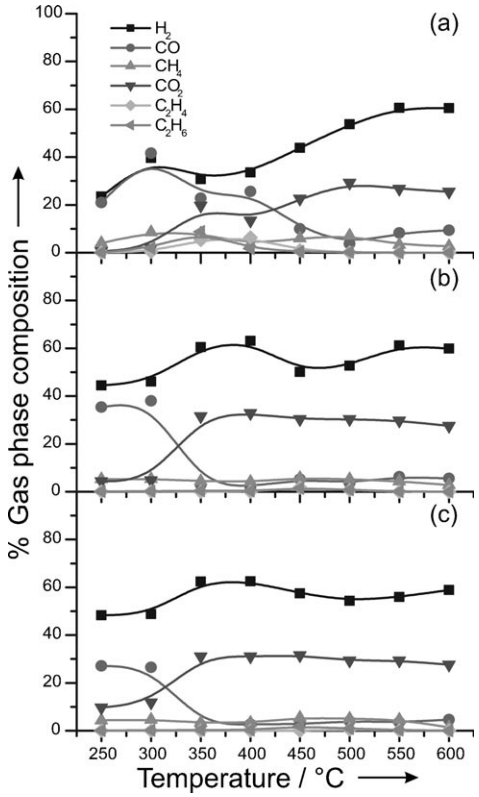

Figure 2. Gas-phase composition as a function of the catalyst temperature on (a) Pt/Al_2O_3, (b) $Pt/La_2O_3/Al_2O_3$, and (c) $Pt/CeO_2/Al_2O_3$ (c). Condition: 1.00 g catalyst, 0.32 mL min^{-1} $C_3H_8O_3$ (30 wt%; aqueous solution).

ol-to-syngas conversion in the 350–400 °C range (Figure 1a). At the same time, very low gas flows were generally recorded (ca. 25 mL min^{-1}) and a significant amount of hydrocarbons (CH_4, C_2H_4, and C_2H_6) was detected in the effluents (Figure 2a). Finally, the collected liquid fraction had a typical yellow–brownish color, suggesting the formation of heavy oxygenated hydrocarbons by condensation side-reactions. A qualitative GC-MS analysis of the liquid fractions collected during the reaction at 350–400 °C confirmed the presence of high levels of unreacted glycerol and evidenced the presence of a large number of byproducts. The most abundant were hydroxyacetone, 1,2-propanediol, ethylene glycol, and their monoesthers with acetic acid. The presence of acrolein or acrilic acid could not be excluded, because the unequivocal attribution of all peaks in the chromatogram was not possible due to the large number of byproducts (present at trace levels). Other authors have observed a similarly low activity for catalytic Pt nanoparticles on carbon supports.[25] This effect was ultimately attributed to a rapid CO passivation of the catalyst active sites already at low temperatures. The passivation of metal sites by CO favors glycerol dehydration at the acidic sites of the support, ultimately increasing the amount of undesired byproducts. A strong increase of the conversion of glycerol into syngas was observed on the same catalyst by increasing the reaction temperature, although complete conversion was never reached. H_2 and CO_2 were produced above 450 °C with the presence of a small amount of CH_4 and CO (> 550 °C).

The poor activity of the Pt/Al_2O_3 catalyst towards glycerol SR can be described as the result of a complex network of side reactions, including dehydration, condensation, and polymerization reactions, promoted by the acid sites of the support as well as dehydrogenation and hydrogenation reactions promoted by the Pt nanoparticles. Comparable results have recently been reported for SR of glycerol by Al_2O_3-supported Ni catalysts[44] as well as for aqueous-phase reforming over Al_2O_3-supported Pt catalysts.[21,58]

Pt/Al_2O_3 catalysts doped with either CeO_2 or La_2O_3 exhibited very different catalytic activities and selectivities. Although a trend similar to Pt/Al_2O_3 was observed at temperatures lower than 300 °C, a sharp increase between 350–400 °C was observed with the doped systems, leading to glycerol conversions close to 100% (Figure 1b and c). While temperatures up to 300 °C generated H_2 and CO [suggesting glycerol decomposition as the main operative process, Equation (2)], a significant increase in H_2 and CO_2 production was observed at temperatures over 350 °C, indicating that the WGS equilibrium [Equation (3)] was also operative (Figure 2). CH_4 was the major byproduct observed, while only traces of C_2H_4 and C_2H_6 were present.

A decrease of the gas flow was observed at temperatures over 400 °C. A similar effect of La_2O_3 and CeO_2 has already been reported by Iriondo et al.,[49] who studied the effect of various doping agents on the activity of Ni/Al_2O_3 catalyst in glycerol SR and APR. While $Pt/CeO_2/Al_2O_3$ showed a decrease up to 500 °C, where glycerol conversion stabilized at around 50%, the $Pt/La_2O_3/Al_2O_3$ system was characterized by a second maximum at around 550 °C, which only marginally affected the final gas stream composition. For both doped catalysts only a slight increase of the CO concentration was observed at higher temperatures, which can reasonably be attributed to the exothermic WGS equilibrium. The gas stream profile for $Pt/La_2O_3/Al_2O_3$ (two relative maxima in the glycerol conversion) was perfectly reproducible and was maintained with different batches of fresh catalyst. Such a profile is probably associated with a progressive deactivation–reactivation of the catalytic sites with the catalyst temperature, with no apparent modification of the

 © 2010 Wiley-VCH Verlag GmbH & Co. KGaA, Weinheim

1864564x, 2010, 5, Downloaded from https://chemistry-europe.onlinelibrary.wiley.com/doi/10.1002/cssc.200900243 by CONICET Consejo Nacional de Investigaciones, Wiley Online Library on [07/12/2023]. See the Terms and Conditions (https://onlinelibrary.wiley.com/terms-and-conditions) on Wiley Online Library for rules of use; OA articles are governed by the applicable Creative Commons License

Table 1. Molar ratios of the main gaseous products during glycerol steam reforming experiments.[a]

Sample	Temperature [°C]	H_2/CO	H_2/CO_2	CO/CO_2	CH_4/H_2
Pt/Al_2O_3	250	1.12	36.20	32.37	0.171
	300	0.95	20.18	21.23	0.217
	350	1.35	1.56	1.16	0.262
	400	1.31	2.49	1.91	0.105
	450	4.42	1.94	0.44	0.137
	500	14.52	1.84	0.13	0.134
	550	7.29	2.27	0.31	0.054
	600	6.43	2.37	0.37	0.044
$Pt/La_2O_3/Al_2O_3$	250	1.26	10.28	8.18	0.118
	300	1.21	9.65	7.97	0.116
	350	20.56	1.92	0.09	0.074
	400	33.76	1.92	0.06	0.066
	450	9.65	1.65	0.17	0.114
	500	14.54	1.74	0.12	0.099
	550	9.82	2.06	0.21	0.071
	600	10.71	2.18	0.20	0.047
$Pt/CeO_2/Al_2O_3$	250	1.78	4.97	2.79	0.090
	300	1.84	4.15	2.26	0.095
	350	26.79	2.01	0.07	0.054
	400	23.14	2.01	0.09	0.054
	450	21.14	1.82	0.09	0.094
	500	13.58	1.86	0.14	0.094
	550	15.75	1.91	0.12	0.083
	600	12.62	2.13	0.17	0.024

[a] Conditions: 1.00 g catalyst, 0.32 mL min^{-1} $C_3H_8O_3$ (30 wt%) water solution.

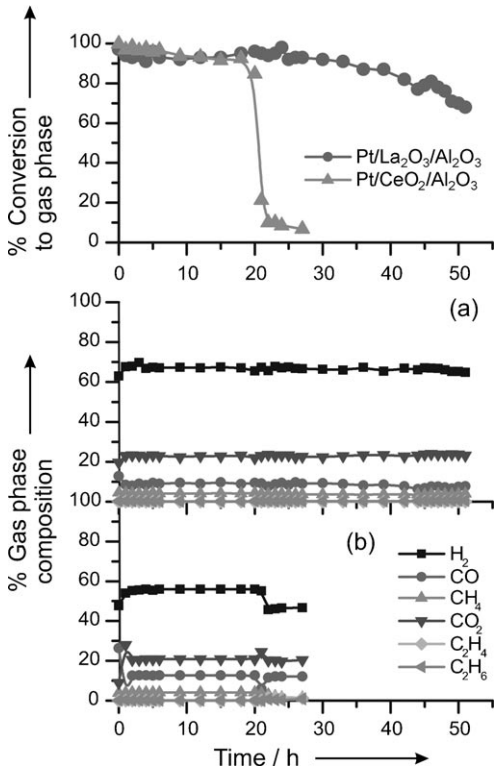

Figure 3. Stability tests over doped Pt/Al_2O_3 catalyst. Top: glycerol conversion to gas-phase products. Bottom: gas-phase composition using (a) $Pt/La_2O_3/Al_2O_3$ and (b) $Pt/CeO_2/Al_2O_3$. Conditions: 1.00 g catalyst, 0.32 mL min^{-1} of $C_3H_8O_3$ (30 wt%; aqueous solution), $T = 350\,^{\circ}C$.

catalyst selectivity. Accordingly, with doped Pt/Al_2O_3 catalysts detectable amounts of unreacted glycerol and byproducts were invariably identified by GC-MS analysis of the liquid fractions collected from the reactor working at temperatures higher than 450 °C

Table 1 presents the evolution of the relative ratios of the main gaseous products, for the various catalysts at different temperatures. The highest CH_4/H_2 ratio was observed with Pt/Al_2O_3, confirming that this catalyst is predisposed towards a higher selectivity for hydrocarbon production. For $Pt/La_2O_3/Al_2O_3$, the analysis of the molar ratios confirmed that below 300 °C glycerol decomposition [Equation (2)] was operative (H_2/CO ratio close to the theoretical value of 1.33). When the temperature was increased the WGS reaction was also involved, approaching the complete steam reforming process [Equation (1)] with $H_2/CO_2 \sim 2.33$; at the same time, the CO/CO_2 ratio was strongly reduced. Finally, for $Pt/CeO_2/Al_2O_3$, the occurrence of the WGS reaction at low temperature was confirmed by the ratio $H_2/CO > 1.33$ already at 250 °C.

Addressing the preservation of the catalyst stability throughout a catalytic process is one of the most important goals when designing new catalytic systems. Long-term stability tests were performed to assess the practical use of our Pt-based catalysts. The stability of the doped catalyst samples in the glycerol SR process was studied at 350 °C (Figure 3); the lowest temperature at which the complete conversion of glycerol to H_2 and CO_2 was achieved. Notably, the plain Pt/Al_2O_3 catalyst showed its lowest catalytic performance at the same temperature. Both doped catalysts showed a good stability for at least 20 h. While the $Pt/CeO_2/Al_2O_3$ system showed a very fast decrease of the glycerol-to-syngas conversion after 20 h, the La_2O_3-doped catalyst maintained its high stability over a period of 50 h. Notably, the selectivity towards the different products remained almost constant throughout the reaction.

The sharp decrease observed with the $Pt/CeO_2/Al_2O_3$ catalyst has also been previously reported in the case of Pt/Al_2O_3.[25] This was interpreted based of the fact that the reactor initially operated at 100% conversion, with glycerol present only in the upstream portion of the catalyst bed in the tubular reactor. Therefore, the deactivation front moves from the reactor inlet to the outlet as olefinic species are formed from glycerol on the Al_2O_3 acid sites, followed by deposition of coke from these species covering the Pt surface sites.[25]

Despite the relatively high ceria loadings (20 wt%), the catalyst surface still presented a significant number of acidic sites [see NH_3 temperature-programmed desorption (TPD) section below]. This may be due to partial agglomeration of ceria into relatively small but appreciable nanoparticles caused by calcination at 700 °C. Indeed, the formation of ceria particles with idealized cubic shapes having edges of ca. 4.3 nm (see XRD section below) would result in a surface area of around 7 m^2 g^{-1}, which corresponds to less than 8% of the total catalyst surface area. By contrast, the very strong dispersion of the basic oxide La_2O_3 resulted in a more significant reduction of the number of acidic Al_2O_3 sites in that system.

 © 2010 Wiley-VCH Verlag GmbH & Co. KGaA, Weinheim

1864564x, 2010, 5, Downloaded from https://chemistry-europe.onlinelibrary.wiley.com/doi/10.1002/cssc.200900243 by CONICET Consejo Nacional de Investigaciones, Wiley Online Library on [07/12/2023]. See the Terms and Conditions (https://onlinelibrary.wiley.com/terms-and-conditions) on Wiley Online Library for rules of use; OA articles are governed by the applicable Creative Commons License

Characterization of fresh catalysts

Temperature programmed reduction (TPR) profiles of the investigated samples are presented in Figure S1 (Supporting Information). All samples containing Pt featured a broad reduction process with a maximum at around 120 °C, related to the reduction of PtO_x species formed during the calcination treatment. While $Pt/CeO_2/Al_2O_3$ showed a significant H_2 consumption above 500 °C due to the bulk reduction of CeO_2, the Pt/Al_2O_3 and $Pt/La_2O_3/Al_2O_3$ samples did not show any reduction processes above 400 °C.

Different types of PtO_x species can be obtained from the oxidation of Pt/Al_2O_3 catalysts,[59] ranging from oxygen-passivated Pt particles (when the oxidation is performed at room temperature) to $PtAl_2O_4$ (by heating Pt nanoparticles in the presence of Al_2O_3 above 600 °C). In our systems the calcination step at 500 °C was expected to simply generate PtO_2, although the high nanoparticle dispersion did not allow a definitive confirmation of the structure of the Pt species (XRD; data not shown). Under a H_2 stream PtO_2 reduction should occur almost quantitatively between 100 and 300 °C, depending on the metal loading, the nature of the support, and the metal dispersion.[59–63] Catalyst pretreatment in a H_2 flow at 500 °C was carried out on all our catalytic systems before characterization and use in glycerol SR. This treatment was expected to completely reduce all Pt species present in the samples.

Physi- and chemisorption experiments carried out on the reduced samples are summarized in Table 2. All samples showed high surface areas and similar pore dimensions, consistent with the texture of the Al_2O_3 support. Introducing doping oxides onto the Al_2O_3 support resulted in a slight decrease of the cumulative pore volume, which was more pronounced in the case of CeO_2 because of a higher doping oxide loading. Such a trend, together with no significant variation of either the specific surface area (SSA) or the pore diameters, indicates a good dispersion of the doping agents on the support surface. H_2 chemisorption finally revealed a high dispersion of the Pt nanoparticles on the supports. A lower H/Pt ratio was observed for the $Pt/CeO_2/Al_2O_3$ sample after reduction at 500 °C, probably because of a partial electronic deactivation of the Pt nanoparticles as previously reported for related CeO_2-based systems.[64] A mild oxidative treatment was applied to the latter sample in order to reoxidize CeO_2 without modifying the Pt dispersion, and to make the H/Pt ratio comparable to those observed for the other samples.

The X-ray diffraction (XRD) pattern of each sample showed signals typical of the θ-Al_2O_3 catalyst support (Figure 4).[65] While the $Pt/CeO_2/Al_2O_3$ catalyst exhibited reflections that could be ascribed to a cubic CeO_2 phase, the $Pt/La_2O_3/Al_2O_3$ system did not show any reflections clearly attributable to specific La-containing species, probably because of the low amount of La_2O_3 or the strong dispersion of the oxide on the support (or a combination of these). Crystallite sizes of 4.3 ± 0.4 nm could be calculated for the activated $Pt/CeO_2/Al_2O_3$ catalyst from XRD profile fitting of the CeO_2 phase. Such a result indicates that the catalyst activation protocol did not affect the structural characteristics of the doping agent.

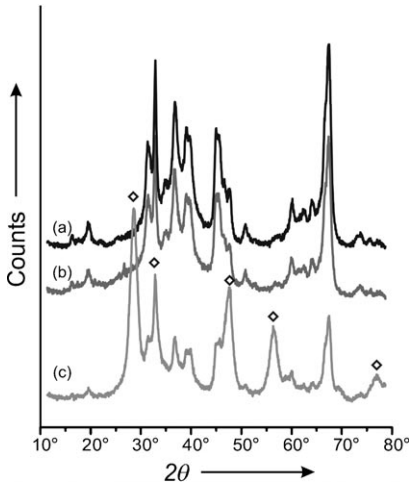

Figure 4. Powder XRD patterns for the samples reduced at 500 °C. (a) Pt/Al_2O_3, (b) $Pt/La_2O_3/Al_2O_3$, and (c) $Pt/CeO_2/Al_2O_3$. CeO_2 reflections are marked by diamonds.

The XRD characterization of supported Pt nanoparticles is generally a difficult task when complex support patterns are combined with a low and broadened pattern of the metal phase. In any case, an accurate study can be performed through comparing the support and catalyst patterns by a Rietveld procedure.[66] To separate the platinum scattering from that of the support, the air-corrected diffraction pattern of the catalyst was fitted through Rietveld methods using a platinum face-centered cubic (fcc) structure and the experimental dif-

Table 2. Physisorption and chemisorption results for the fresh catalysts.

Sample	SSA[a] [$m^2 g^{-1}$]	d_M[b] [nm]	CPV[c] [$mL g^{-1}$]	H/Pt[d]	PS[e] [nm]	CS[f] [nm]
Al_2O_3	97	11	0.367	–	–	–
Pt/Al_2O_3	96	11	0.349	0.75	1.4	1.5
La_2O_3/Al_2O_3	91	12	0.338	–	–	–
$Pt/La_2O_3/Al_2O_3$	89	11	0.323	0.68	1.6	1.5
CeO_2/Al_2O_3	100	11	0.292	–	–	–
$Pt/CeO_2/Al_2O_3$	96	11	0.281	0.48 0.73[g]	2.3 1.6[g]	– –

[a] Specific surface area, from Brunauer–Emmett–Teller (BET) analysis. [b] Maximum of the Barrett–Joyner–Halenda (BJH) pore distribution calculated from the desorption branch. [c] Cumulative pore volume. [d] H/Pt ratio obtained from H_2 chemisorption at −94 °C of the samples previously reduced at 500 °C for 5 h. [e] Average Pt particle size obtained from H_2 chemisorption assuming a spherical geometry. [f] Average Pt crystallite size determined by XRD. [g] After reduction at 500 °C, the sample was oxidized at 427 °C by flowing O_2 (5%)/Ar (30 mL min^{-1}), then reduced at 100 °C by flowing H_2 (5%)/Ar (30 mL min^{-1}), and finally evacuated at 400 °C for 4 h according to Ref. [64].

© 2010 Wiley-VCH Verlag GmbH & Co. KGaA, Weinheim

1864564x, 2010, 5, Downloaded from https://chemistry-europe.onlinelibrary.wiley.com/doi/10.1002/cssc.200900243 by CONICET Consejo Nacional de Investigaciones, Wiley Online Library on [07/12/2023]. See the Terms and Conditions (https://onlinelibrary.wiley.com/terms-and-conditions) on Wiley Online Library for rules of use; OA articles are governed by the applicable Creative Commons License

fraction pattern of the support. This analytical method allows for a quantitative evaluation of the metal phase as well. In this way, an additional internal validity test of the line broadening analysis is performed (Figures S2–S4).[67] The main Pt crystallite sizes are listed in Table 2. Pt crystallite sizes of 1.5 ± 0.2 nm were calculated for both Pt/Al_2O_3 and $Pt/La_2O_3/Al_2O_3$, in good agreement with the H_2 chemisorption experiments. Similar to $Pt/CeO_2/Al_2O_3$, the low-quality separation of the XRD pattern of the metallic phase from that of the CeO_2/Al_2O_3 support did not allow for an accurate determination of the Pt nanoparticle distribution (Figure S4). Moreover, the Rietveld refinement of the XRD pattern for the reduced $Pt/CeO_2/Al_2O_3$ species accounted for a Pt loading of ca. 5.5 wt%, which is almost double the nominal amount of Pt. This is further proof of the low-quality evaluation of the Pt XRD pattern of this material. By contrast, Pt contents of 2.7 wt% and 2.3 wt% were obtained for Pt/Al_2O_3 and $Pt/La_2O_3/Al_2O_3$, respectively, which fitted well with the nominal Pt loadings (3 wt%). The low quality of the XRD diffractograms of the active phase of $Pt/CeO_2/Al_2O_3$ can be attributed to the high scattering factor of CeO_2, the reflections of which dominate the XRD pattern. Finally, the lack of clear metallic Pt reflections in all samples suggests a very strong dispersion of Pt nanoparticles (dimension <1 nm) on the surface of the catalyst, in agreement with the H_2 chemisorption results.

The acidity of the different catalysts were determined by NH_3-TPD. NH_3 desorption from Al_2O_3-based materials is usually reported in the range between 100–500 °C for NH_3 adsorbed on Brønsted-acidic sites (OH groups).[68] As Figure 5 shows, La_2O_3 or CeO_2 doping had a strong effect on the population of acidic sites and, consequently, on the adsorbed amount of NH_3. Pt/Al_2O_3 adsorbed the largest amount of NH_3. At least two superimposed desorption peaks can be identified (ca. 220 and ca. 325 °C), related to weakly and medium–strongly adsorbed NH_3. The introduction of La_2O_3 and CeO_2 resulted in a strong reduction of the amount of desorbed NH_3, together with a significant shift to lower temperatures for both desorption maxima. Because comparable surface areas were measured for all samples, these results indicate that the addition of basic promoters reduces the number of acidic sites and their strength. The significantly lower acidity of the La_2O_3-based system can be explained by the very high dispersion of the doping oxide on the alumina surface.

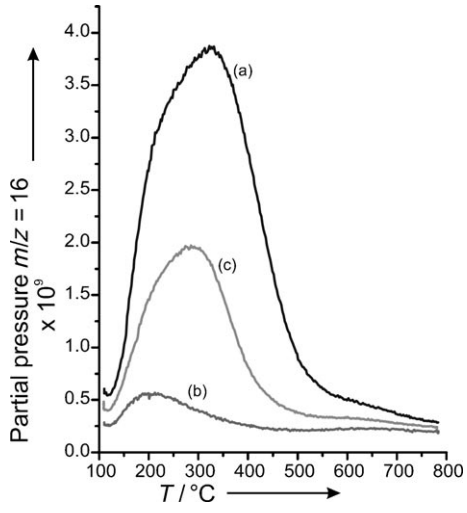

Figure 5. NH_3-TPD profiles recorded for samples reduced at 500 °C. (a) Pt/Al_2O_3, (b) $Pt/La_2O_3/Al_2O_3$, and (c) $Pt/CeO_2/Al_2O_3$.

The reduced acidity of the materials promoted by La_2O_3 and CeO_2 doping explains their better performance in the glycerol SR. The lower reforming activity observed with Pt/Al_2O_3 is therefore ascribed to the occurrence of an undesired dehydration/condensation side reaction catalyzed by the acid sites of the support.

Effect of CeO_2 and La_2O_3 doping on catalyst stability and origin of deactivation effects

Exhausted catalysts, as obtained after aging under glycerol SR conditions, were fully characterized in an attempt to reveal possible structural modifications as well as deactivation phenomena that occurred during the catalytic process. Table 3 summarizes the results of physi- and chemisorption experiments performed on the aged samples. A significant reduction of the number of accessible Pt active sites is evident. This effect may be due to the concomitant occurrence of several processes: (1) partial sintering of the Pt nanoparticles, (2) deposition of carbonaceous residues onto the Pt active sites (coke), and (3) progressive occlusion of the pores onto the catalyst support.

Table 3. Physisorption and chemisorption results for the aged catalysts.

Sample	SSA[a] [$m^2 g^{-1}$]	d_M[b] [nm]	CPV[c] [$mL g^{-1}$]	H/Pt[d]	PS[e] [nm]	CS[f] [nm]
Pt/Al_2O_3 run-up at 600 °C	78	15	0.268	0.35	3.2	3.0
$Pt/La_2O_3/Al_2O_3$ run-up at 600 °C	69	17	0.161	0.32	3.6	2.7
$Pt/La_2O_3/Al_2O_3$ Stability at 350 °C	80	16	0.270	0.21	5.3	2.2
$Pt/CeO_2/Al_2O_3$ run-up at 600 °C	78	15	0.234	0.42	2.7	n.d.[g]
$Pt/CeO_2/Al_2O_3$ Stability at 350 °C	95	16	0.276	0.48	2.4	n.d.[g]

[a] Specific surface area from BET analysis. [b] Maximum of the BJH pore distribution calculated from the desorption branch. [c] Cumulative pore volume. [d] H/Pt ratio obtained from H_2 chemisorption at −94 °C of the samples previously reduced at 500 °C for 5 h. [e] Average Pt particle size obtained from H_2 chemisoprtion assuming a spherical geometry. [f] Average Pt crystallite size determined by powder XRD. [g] Not determined.

The latter point was confirmed by N_2 physisorption experiments, in which a progressive decrease of the specific surface areas and pore volumes was recorded for all aged samples. Calculation of the Pt nanoparticle sizes from XRD patterns (Figure 6) of the aged catalysts (after subtracting the support contribution) showed an appreciable increase of the Pt nanoparticle dimensions of both Pt/Al_2O_3 and $Pt/La_2O_3/Al_2O_3$ (Figures S5 and S6). This result fits well with the H_2 chemisorption

 © 2010 Wiley-VCH Verlag GmbH & Co. KGaA, Weinheim

1864564x, 2010, 5, Downloaded from https://chemistry-europe.onlinelibrary.wiley.com/doi/10.1002/cssc.200900243 by CONICET Consejo Nacional de Investigaciones, Wiley Online Library on [07/12/2023]. See the Terms and Conditions (https://onlinelibrary.wiley.com/terms-and-conditions) on Wiley Online Library for rules of use; OA articles are governed by the applicable Creative Commons License

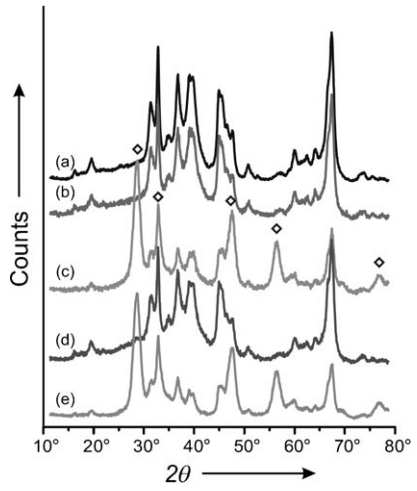

Figure 6. Powder XRD patterns of the aged samples. (a) Pt/Al_2O_3, (b) $Pt/La_2O_3/Al_2O_3$, and (c) $Pt/CeO_2/Al_2O_3$ after run-up activity up to 600 °C. (d) $Pt/La_2O_3/Al_2O_3$ and (e) $Pt/CeO_2/Al_2O_3$ after stability tests at 350 °C for 52 and 27 h, respectively. The reflections of CeO_2 are marked by diamonds.

experiments. The decrease of the H/Pt values can be explained by the occurrence of effects (1) and (2) mentioned above.

Thermogravimetric analysis (TGA) of the exhausted catalysts allowed an assessment of both the amount and type of carbonaceous compounds deposited onto the catalyst surface. Coupling TGA with a quadrupole MS gas analysis of the volatiles finally provided a clear identification of the decomposition products (basically H_2O and CO_2). The TGA profiles and the curves related to CO_2 evolution are reported in Figure 7. From closer inspection of Table 2, Table 3, and Figure 7, it can be concluded that both metal sintering and coke deposition were operative in all catalytic tests.

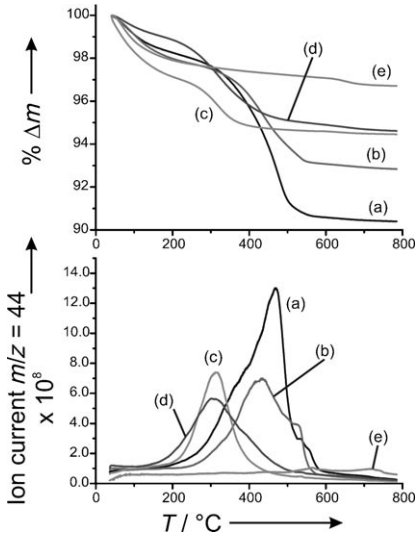

Figure 7. (Top) Weight loss and (bottom) CO_2 evolution revealed during TGA-MS analysis of the aged samples (air, 50 mL min^{-1}). (a) Pt/Al_2O_3, (b) $Pt/La_2O_3/Al_2O_3$, and (c) $Pt/CeO_2/Al_2O_3$ after run-up activity up to 600 °C. (d) $Pt/La_2O_3/Al_2O_3$ and (e) $Pt/CeO_2/Al_2O_3$ after stability tests at 350 °C for 52 and 27 h, respectively.

H_2O evolution, due to humidity adsorbed at the catalyst surface (unreported data) with no concomitant CO_2 formation and responsible for the initial catalyst weight loss, was observed below 200 °C for all the analyzed samples. Above 200 °C, carbonaceous deposits started to burn, with the production of only marginal amounts of H_2O. As Figure 7 shows, Pt/Al_2O_3 exhibited the highest weight loss (6.4 wt%), with a significant CO_2 evolution between 250 and 600 °C. This observation is perfectly in line with its lower catalytic activity. A high amount of carbonaceous compounds actually covers the catalyst surface during the reforming process, as a consequence of the higher acidity of the catalyst support. By contrast, $Pt/La_2O_3/Al_2O_3$ and $Pt/CeO_2/Al_2O_3$ showed significantly lower amounts of adsorbed organic residues (4.1 wt% and 1.9 wt%, respectively). These lower amounts of carbonaceous deposits can ultimately be related to the lower acidities of the catalyst supports.[25,69] Similar CO_2 evolution profiles and comparable temperature ranges for $Pt/La_2O_3/Al_2O_3$ and Pt/Al_2O_3 suggested a similar nature of the carbonaceous deposits. On the other hand, the $Pt/CeO_2/Al_2O_3$ sample showed a symmetric CO_2 evolution peak in a lower temperature range. This result can be reasonably ascribed to either a less graphitic nature of the coke deposits and/or to a cooperative effect of CeO_2 in the combustion of the carbonaceous materials. In fact, it is well-known that the introduction of CeO_2-based addictives to a reforming catalyst can prevent the deposition of coke-based materials or favor their elimination during oxidative treatments.[35,38]

Prolonged reactivity tests at 350 °C with both $Pt/La_2O_3/Al_2O_3$ and $Pt/CeO_2/Al_2O_3$ revealed the formation of a small amount of carbonaceous deposits, suggesting that a higher catalyst temperature leads to a higher amount of coke deposits. For the $Pt/La_2O_3/Al_2O_3$ catalyst, a lower reaction temperature reduced the polymerization reaction (weight loss 3.3 wt%), leading to carbonaceous deposits that were easily removed during TGA (Figure 7d). Finally, despite the profound and sudden loss of reforming activity, very low amounts of carbonaceous deposits were removed during the TGA analysis (weight loss ca. 0.5 wt %) around 600–700 °C (Figure 7e).

Figure 8 shows representative high-resolution (HRTEM) images acquired from the spent $Pt/La_2O_3/Al_2O_3$ catalyst after stability test under glycerol SR conditions at 350 °C for 52 h. Pt nanoparticles can easily be recognized in the images as dark particles and by their spacing between lattice planes (0.23 nm vs. 0.226 nm for the (111) reflection of Pt). The dimensions of the Pt nanoparticles are in the 2–3 nm range, in good agreement with XRD, and the size of the nanoparticles was only marginally affected by their prolonged use under glycerol SR conditions.

Energy-dispersive X-ray (EDX) analysis confirmed the presence of lanthanum, although no clear attribution to a particular phase was possible (as also found by XRD).The Al_2O_3 support appears in the HRTEM images as well-defined crystallites with dimensions of 15–20 nm. Some examples of relatively clean particles of the support are present in the upper part of Figure 8, where the lattice plane of θ-Al_2O_3 can be observed (0.26 nm vs. 0.256 nm for the $(11\bar{1})$ reflection of θ-Al_2O_3).

 © 2010 Wiley-VCH Verlag GmbH & Co. KGaA, Weinheim

1864564x, 2010, 5, Downloaded from https://chemistry-europe.onlinelibrary.wiley.com/doi/10.1002/cssc.200900243 by CONICET Consejo Nacional de Investigaciones, Wiley Online Library on [07/12/2023]. See the Terms and Conditions (https://onlinelibrary.wiley.com/terms-and-conditions) on Wiley Online Library for rules of use; OA articles are governed by the applicable Creative Commons License

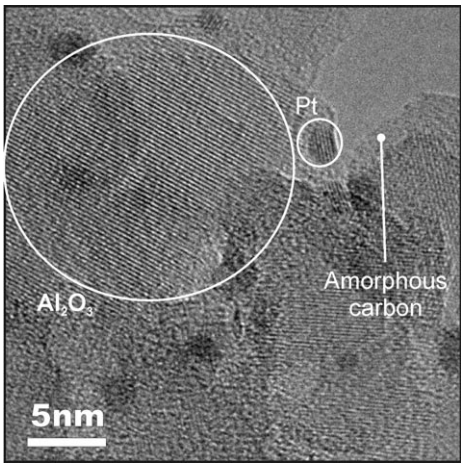

Figure 8. Representative HRTEM image of a $Pt/La_2O_3/Al_2O_3$ after stability tests at 350 °C for 52 h.

Some carbonaceous amorphous regions of a few nanometers were observed on the surface of the used catalyst. However, suitable information about the spatial distribution of carbon species on the active particles could not be unambiguously determined. Despite this, the reduction of the H/Pt ratio measured by H_2 chemisorption suggested that the amorphous carbon deposits partially covered the Pt nanoparticles, because the real dimension of the nanoparticles was only marginally affected by their prolonged use under glycerol SR (as evidenced by XRD and HRTEM).

Conclusions

The present study deals with the effects that result from the addition of basic oxides (La_2O_3 and CeO_2) to Pt/Al_2O_3 catalysts for the H_2 production through glycerol steam reforming. The most relevant conclusions of this work can be summarized as follows:

(1) Pt/Al_2O_3 catalysts promote H_2 production only at high temperatures (> 500 °C), which results from side reactions promoted by acidic sites on the Al_2O_3 support. Many undesired byproducts formed by dehydration–polymerization reactions were detected in the liquid effluent of the reactor.

(2) La_2O_3 and CeO_2 deposited onto Al_2O_3 improve the catalytic performances of the Pt nanoparticles by decreasing the acidity of the support, as evidenced by NH_3-TPD. Such a metal oxide doping allows glycerol to be completely converted into syngas already at 350 °C. efficiently promoting, at the same time, the water–gas shift reaction. Finally, small amounts of CH_4 are produced as a result of concomitant hydrogenation reactions.

(3) The addition of La_2O_3 and CeO_2 significantly improves the catalyst stability as a consequence of the reduced acidity of the Al_2O_3 support. Moreover, the amount of carbon deposits is significantly reduced compared to the plain Pt/Al_2O_3 sample. Despite these positive effects, the CeO_2-doped catalyst deactivates quickly after 20 h at 350 °C while a higher stability is shown by the La_2O_3-doped sample (over 50 h).

(4) The detailed characterization of the fresh and spent catalysts allowed a better understanding of our doped catalysts behavior under glycerol SR conditions. The slight deactivation observed for $Pt/La_2O_3/Al_2O_3$ catalyst can be related to coke deposition on the catalyst surface, resulting in a significant coverage of Pt (as assessed by H_2 chemisorption and HRTEM). The effect of Pt sintering or surface area decrease is only marginal.

Experimental Section

Catalyst preparation

All studied catalysts were supported on Al_2O_3 beads to reduce the overpressure inside the reactor during activity tests. Al_2O_3 (Puralox TH100) beads were kindly provided by SASOL in the form of spheres (diameter ca. 1.0 mm) and were calcined at 900 °C for 24 h before use to remove all organic binders and stabilize their texture. The beads were modified by introducing either La_2O_3 or CeO_2 to reduce the catalyst support acidity and evaluate (in the case of CeO_2) the effects of the presence of a redox-active component. La_2O_3 (5 wt%) was introduced by impregnation of the Al_2O_3 spheres using a solution of $La(NO_3)_3{\cdot}9H_2O$ in water. Afterwards, the solvent was removed by evaporation at reduced pressure and the resulting material was dried at 120 °C overnight and calcined in static air at 700 °C for 5 h. CeO_2 (20wt%) was introduced by impregnation of the Al_2O_3 spheres (previously degassed at 225 °C overnight) using an isooctane solution of $Ce(OC_8H_{17})_4$. The latter was prepared according to literature procedures.[70] After soaking of the Al_2O_3 spheres, the solvent was removed by evaporation at reduced pressure and the resulting material was dried at 120 °C overnight and calcined in static air at 700 °C for 5 h. The amounts of La_2O_3 and CeO_2 were optimized in order to introduce the maximum quantity of the dopant oxide without significant variations of the support surface area (see Table 2). Pt (3 wt%) was loaded on the bare or modified Al_2O_3 spheres by impregnation using an aqueous solution of $Pt(NO_3)_2$. After drying at 120 °C overnight, the products were calcined at 500 °C for 5 h.

Catalytic activity

In a typical procedure, 1 g of fresh catalyst was loaded over fused SiO_2 granules (−4 + 16 mesh; Sigma–Aldrich), in the middle of a $^1/_4$-inch outer diameter stainless-steel reactor placed in an electrical furnace. Fused SiO_2 granules were then used to cover the catalytic bed to favor the vaporization of liquid reagents injected from the top of the reactor. A type-K thermocouple was finally attached to the outside of the reactor to measure its temperature. Fresh catalysts were reduced before each catalytic test by treatment with pure H_2 (25 mL min^{-1}) at 500 °C for 5 h. After purging the reactor with Ar and cooling to the desired temperature, an aqueous solution of glycerol (30 wt%) was introduced at its top by means of a KNF pump (Model STEPDOS 03 RC), which allowed for a constant flow rate of 0.32 mL min^{-1} throughout the catalytic process. The outlet effluents were cooled through a water condenser to remove all liquid fractions. Volatiles were analyzed online by GC using a Hewlett Packard 6890 gas chromatograph and then vented. A Molsieve 5 A column, using Ar as carrier, connected to a thermal conductivity detector (TCD) was used to follow the H_2, O_2, N_2, CH_4, and CO production. A PoraPLOT Q column, using He as carrier, connected to both a methanator and a flame ionization detector (FID) was used to analyze all carbon-containing compounds.

 © 2010 Wiley-VCH Verlag GmbH & Co. KGaA, Weinheim

1864564x, 2010, 5, Downloaded from https://chemistry-europe.onlinelibrary.wiley.com/doi/10.1002/cssc.200900243 by CONICET Consejo Nacional de Investigaciones, Wiley Online Library on [07/12/2023]. See the Terms and Conditions (https://onlinelibrary.wiley.com/terms-and-conditions) on Wiley Online Library for rules of use; OA articles are governed by the applicable Creative Commons License

After reducing all catalysts at 500 °C, the systems were cooled to 250 °C and the liquid injection started. The catalyst temperature was maintained at 250 °C for 1 h before starting GC analysis. Afterwards, the catalyst temperature was increased step-by-step up to 600 °C (steps of 50 °C), and volatiles produced at the reactor outlet were systematically analyzed throughout the whole temperature range. For stability tests, after the reduction step, the systems were cooled to the final temperature (350 °C), at which stage the injection of the glycerol solution and the GC analysis of volatiles produced at the reactor outlet started.

Catalysts characterization

All catalysts were fully characterized with respect to their morphological and structural properties, both as freshly prepared systems and as aged catalysts (run-up test up to 600 °C and stability test at 350 °C). H_2 chemisorption and physisorption measurements were conducted using a Micromeritics ASAP 2020 analyzer. N_2 physisorption isotherms were collected at −196 °C on 0.1 g of sample, after evacuation at 350 °C overnight. Surface areas and pore distributions were obtained applying the Brunauer–Emmett–Teller (BET) and Barrett–Joyner–Halenda (BJH) models, respectively. H_2 chemisorption experiments were conducted at −94 °C (solid/liquid acetone bath) on 0.2 g of catalyst. The calcined samples were pre-reduced in a flow of H_2 (35 mL min^{-1}) at a heating rate of 10 °C min^{-1} up to 500 °C (standard activation temperature). After 5 h at this temperature, the samples were evacuated at 400 °C for 4 h, and cooled under vacuum to the adsorption temperature (−90 °C). Typically, an equilibration time of 10 min was employed. Adsorbed volumes were determined by extrapolation to zero pressure of the linear part of the adsorption isotherm (100–400 torr) after elimination of reversible hydrogen adsorption. A chemisorption stoichiometry H/Pt = 1:1 was assumed. Aged samples were not subjected to standard cleaning procedures to avoid metal redispersion and/or carbonaceous species removal. These samples were pre-reduced for 1 h in a flow of H_2 (5 %)/Ar (35 mL min^{-1}) at a heating rate of 10 °C min^{-1} up to 100 °C, evacuated at 400 °C for 4 h, and subjected to chemisorption measurement at −90 °C.

A Philips X'Pert vertical goniometer with Bragg–Brentano geometry, connected to a highly stabilized generator, was used for XRD measurements. A focusing graphite monochromator and a proportional counter with a pulse-height discriminator were used. Nickel-filtered Cu Kα radiation and a step-by-step technique were employed (steps of $2\theta = 0.05°$), with collection times of 10 s step^{-1}. Line broadening analysis (LBA) was carried out using a previously published method.[71] The quantitative phase analysis by X-ray diffraction was performed using the Rietveld method (DBWS9600 computer program written by Sakthivel & Young and modified by Riello et al.).[72]

TPR was performed on 0.1 g of the calcined materials. The samples were pretreated at 500 °C for 1 h by pulsing 100 μL of O_2 in an Ar flow every 75 s, then purged with Ar at 150 °C for 15 min, and cooled to RT. H_2 (5 %)/Ar was admitted into the reactor and the flow allowed to stabilize for 30 min before increasing the temperature to 1000 °C at 10 °C min^{-1}. After TPR, the samples were outgassed under an Ar flow at 1000 °C for 15 min and cooled to 427 °C, at which temperature oxidation was carried out with pulses of O_2 in an Ar flow for 1 hour. H_2 consumption was monitored using a TCD.

TPD of ammonia was conducted in a home-made flow apparatus using a mass spectrometer Hiden HPR20 as analyzer. In a typical NH_3 TPD experiment, about 0.25 g of the sample was loaded in a U-shaped quartz microreactor. The samples were reduced by flowing H_2 (25 mL min^{-1}) at 500 °C for 5 h. After the treatment, the adsorbed H_2 was removed by flowing the system with Ar at 500 °C for 30 min. Afterwards, the samples were cooled at 110 °C under an inert gas flow. For NH_3 adsorption, the reduced samples were saturated by flowing NH_3 (10 %)/Ar (50 mL min^{-1}) at 110 °C for 30 min. After NH_3 adsorption, the sample was flushed in Ar flow at 110 °C for 1 h to remove physically adsorbed NH_3. The NH_3 TPD profile of each sample was recorded by increasing the temperature from 110 to 800 °C with a heating rate of 10 °C min^{-1} under flow of Ar (50 mL min^{-1}). The desorbed products were analyzed by means of a mass spectrometer operating in electron impact mode with a ionization energy of 35 eV. The desorbed species were identified on the basis of the intensity of various mass fragments. In particular, the peak $m/z = 16$ was used to follow the evolution of ammonia because the parent peak ($m/z = 17$) was influenced by the desorbed water.

The carbon deposits on the aged catalysts were characterized by using TGA analysis, performed by using a EXSTAR Thermo Gravimetric Analyzer (TG/DTA) Seiko 6200 coupled with a mass spectrometer ThermoStar GSD 301 T for the analysis of the exhaust gases. Typically, 20 mg of the aged samples were loaded in the instrument and the TGA was performed in flowing air (flow rate 100 mL min^{-1}) with a heating rate of 10 °C min^{-1}.

HRTEM images were collected on representative samples with a Jeol 3010 high resolution electron microscope (1.7 nm point-to-point) operating at 300 keV using a Gatan slow-scan CCD camera (mod. 794). The samples were suspended in hexane and a single drop was placed on a 200-mesh copper carbon-hole grid. Images were collected with a magnification of approximately 600000x.

Acknowledgements

Prof. M. Graziani (University of Trieste, Italy) is gratefully acknowledged for fruitful discussions. Dr. P. Canton (University of Venice, Italy) is gratefully acknowledged for HRTEM investigations. Dr. Werner Oberhauser (ICCOM-CNR, Italy) is gratefully acknowledged for GC-MS analysis. Part of the work has been performed within the ICS-UNIDO program "Next generation of biofuels and biobased chemicals." R.S., P.D., N.B., and P.F. thank ICS-UNIDO for support. SASOL is acknowledged for providing Al_2O_3 spheres. B.L. thanks ACTA SpA for financial support (Ph.D. grant, University of Trieste). The Universities of Trieste and Venice, ICCOM-CNR, INSTM, MIUR (Rome) PRIN2007 Project "Sustainable processes of second generation for H_2 production from renewable sources" are also acknowledged for financial support.

Keywords: biofuels · glycerol · heterogeneous catalysis · platinum · supported catalysts

[1] M. Graziani, P. Fornasiero, *Renewable Resources and Renewable Energy: A Global Challenge*, Taylor & Francis, New York, **2007**.
[2] J. N. Chheda, G. W. Huber, J. A. Dumesic, *Angew. Chem.* **2007**, *119*, 7298; *Angew. Chem. Int. Ed.* **2007**, *46*, 7164.
[3] R. Ramachandran, R. K. Menon, *Int. J. Hydrogen Energy* **1998**, *23*, 593.
[4] S. Adhikari, S. Fernando, S. R. Gwaltney, S. D. Filip To, R. Mark Bricka, P. H. Steele, A. Haryanto, *Int. J. Hydrogen Energy* **2007**, *32*, 2875.
[5] N. Luo, X. Zhao, F. Cao, T. Xiao, D. Fang, *Energy Fuels* **2007**, *21*, 3505.
[6] G. W. Huber, J. A. Dumesic, *Catal. Today* **2006**, *111*, 119.
[7] M. Ni, D. Y. C. Leung, M. K. H. Leung, K. Sumathy, *Fuel Process. Technol.* **2006**, *87*, 461.
[8] C. Sattler, M. Roeb, H. Iler-Steinhagen, *Chem. Eng.* **2007**, 46.

 © 2010 Wiley-VCH Verlag GmbH & Co. KGaA, Weinheim

1864564x, 2010, 5, Downloaded from https://chemistry-europe.onlinelibrary.wiley.com/doi/10.1002/cssc.200900243 by CONICET Consejo Nacional de Investigaciones, Wiley Online Library on [07/12/2023]. See the Terms and Conditions (https://onlinelibrary.wiley.com/terms-and-conditions) on Wiley Online Library for rules of use; OA articles are governed by the applicable Creative Commons License

[9] F. E. Osterloh, *Chem. Mater.* **2008**, *20*, 35.
[10] J. Turner, G. Sverdrup, M. K. Mann, P. C. Maness, B. Kroposki, M. Ghirardi, R. J. Evans, D. Blake, *Int. J. Energy Res.* **2008**, *32*, 379.
[11] R. R. Davda, J. W. Shabaker, G. W. Huber, R. D. Cortright, J. A. Dumesic, *Appl. Catal. B: Environm.* **2005**, *56*, 171.
[12] X. Fu, J. Long, X. Wang, D. Y. C. Leung, Z. Ding, L. Wu, Z. Zhang, Z. Li, X. Fu, *Int. J. Hydrogen Energy* **2008**, *33*, 6484.
[13] V. M. Daskalaki, D. I. Kondarides, *Catal. Today* **2009**, *144*, 75.
[14] D. I. Kondarides, V. M. Daskalaki, A. Patsoura, X. E. Verykios, *Catal. Lett.* **2008**, *122*, 26.
[15] S. Fernando, S. Adhikari, C. Chandrapal, N. Murali, *Energy Fuels* **2006**, *20*, 1727.
[16] M. Kleinert, T. Barth, *Energy Fuels* **2008**, *22*, 1371.
[17] A. Fujishima, K. Honda, *Nature* **1972**, *238*, 37.
[18] L. De Rogatis, P. Fornasiero, in *Catalysis for Sustainable Energy Production* (Eds.: P. Barbaro, C. Bianchini), Wiley, New York, **2009**, pp. 173 – 223.
[19] G. W. Huber, S. Iborra, A. Corma, *Chem. Rev.* **2006**, *106*, 4044.
[20] G. Wen, Y. Xu, H. Ma, Z. Xu, Z. Tian, *Int. J. Hydrogen Energy* **2008**, *33*, 6657.
[21] N. Luo, X. Fu, F. Cao, T. Xiao, P. P. Edwards, *Fuel* **2008**, *87*, 3483.
[22] A. Sivasamy, K. Y. Cheah, P. Fornasiero, F. Kemausuor, S. Zinoviev, S. Miertus, *ChemSusChem* **2009**, *2*, 278.
[23] C. H. Zhou, J. N. Beltramini, Y. X. Fan, G. Q. Lu, *Chem. Soc. Rev.* **2008**, *37*, 527.
[24] A. Brandner, K. Lehnert, A. Bienholz, M. Lucas, P. Claus, *Top. Catal.* **2009**, *52*, 278.
[25] R. R. Soares, D. A. Simonetti, J. A. Dumesic, *Angew. Chem.* **2006**, *118*, 4086; *Angew. Chem. Int. Ed.* **2006**, *45*, 3982.
[26] N. Armaroli, V. Balzani, *Angew. Chem.* **2007**, *119*, 52; *Angew. Chem. Int. Ed.* **2007**, *46*, 52.
[27] A. Corma Canos, S. Iborra, A. Velty, *Chem. Rev.* **2007**, *107*, 2411.
[28] M. Pagliaro, R. Ciriminna, H. Kimura, M. Rossi, C. la Pina, *Angew. Chem.* **2007**, *119*, 4516; *Angew. Chem. Int. Ed.* **2007**, *46*, 4434.
[29] M. Pagliaro, M. Rossi, *Future of Glycerol*, RSC Publishing, London, **2008**.
[30] Y. Zheng, X. Chen, Y. Shen, *Chem. Rev.* **2008**, *108*, 5253.
[31] P. D. Vaidya, A. E. Rodrigues, *Chem. Eng. Technol.* **2009**, *32*, 1463.
[32] S. Adhikari, S. D. Fernando, A. Haryanto, *Energy Convers. Manage.* **2009**, *50*, 2600.
[33] G. W. Huber, J. N. Chheda, C. J. Barrett, J. A. Dumesic, *Science* **2005**, *308*, 1446.
[34] T. Hirai, N. O. Ikenaga, T. Miyake, T. Suzuki, *Energy Fuels* **2005**, *19*, 1761.
[35] S. Adhikari, S. Fernando, A. Haryanto, *Catal. Today* **2007**, *129*, 355.
[36] A. J. Byrd, K. K. Pant, R. B. Gupta, *Fuel* **2008**, *87*, 2956.
[37] P. J. Dauenhauer, J. R. Salge, L. D. Schmidt, *J. Catal.* **2006**, *244*, 238.
[38] B. Zhang, X. Tang, Y. Li, Y. Xu, W. Shen, *Int. J. Hydrogen Energy* **2007**, *32*, 2367.
[39] B. Zhang, X. Tang, Y. Li, W. Cai, Y. Xu, W. Shen, *Catal. Commun.* **2006**, *7*, 367.
[40] S. M. Swami, M. A. Abraham, *Energy Fuels* **2006**, *20*, 2616.
[41] A. M. D. Douette, S. Q. Turn, W. Wang, V. I. Keffer, *Energy Fuels* **2007**, *21*, 3499.
[42] E. L. Kunkes, D. A. Simonetti, J. A. Dumesic, W. D. Pyrz, L. E. Murillo, J. G. Chen, D. J. Buttrey, *J. Catal.* **2008**, *260*, 164.
[43] D. A. Simonetti, E. L. Kunkes, J. A. Dumesic, *J. Catal.* **2007**, *247*, 298.
[44] A. Iriondo, V. L. Barrio, J. F. Cambra, P. L. Arias, M. B. Guemez, R. M. Navarro, M. C. Sanchez-Sanchez, J. L. G. Fierro, *Catal. Commun.* **2009**, *10*, 1275.
[45] M. Slinn, K. Kendall, C. Mallon, J. Andrews, *Bioresour. Technol.* **2008**, *99*, 5851.
[46] S. Adhikari, S. D. Fernando, S. D. F. To, R. M. Bricka, P. H. Steele, A. Haryanto, *Energy Fuels* **2008**, *22*, 1220.
[47] S. Adhikari, S. D. Fernando, A. Haryanto, *Renewable Energy* **2008**, *33*, 1097.
[48] S. Adhikari, S. D. Fernando, A. Haryanto, *Chem. Eng. Technol.* **2009**, *32*, 541.
[49] A. Iriondo, V. L. Barrio, J. F. Cambra, P. L. Arias, M. B. Guemez, R. M. Navarro, M. C. Sanchez-Sanchez, J. L. G. Fierro, *Top. Catal.* **2008**, *49*, 46.
[50] B. Dou, V. Dupont, G. Rickett, N. Blakeman, P. T. Williams, H. Chen, Y. Ding, M. Ghadiri, *Bioresour. Technol.* **2009**, *100*, 3540.
[51] P. O. Sharma, S. Swami, S. Goud, M. A. Abraham, *Environ. Prog.* **2008**, *27*, 22.
[52] G. W. Huber, J. W. Shabaker, J. A. Dumesic, *Science* **2003**, *300*, 2075.
[53] E. C. Wanat, K. Venkataraman, L. D. Schmidt, *Appl. Catal. A: Gen.* **2004**, *276*, 155.
[54] T. Montini, L. De Rogatis, V. Gombac, P. Fornasiero, M. Graziani, *Appl. Catal. B: Environm.* **2007**, *71*, 125.
[55] X. Q. Wang, J. A. Rodriguez, J. C. Hanson, D. Gamarra, A. Martinez-Arias, M. Fernandez-Garcia, *J. Phys. Chem. B* **2006**, *110*, 428.
[56] A. Karpenko, R. Leppelt, V. Plzak, J. Cai, A. Chuvilin, B. Schumacher, U. Kaiser, R. J. Behm, *Top. Catal.* **2007**, *44*, 183.
[57] S. Pradhan, A. S. Reddy, R. N. Devi, S. Chilukuri, *Catal. Today* **2009**, *141*, 72.
[58] K. Murata, I. Takahara, M. Inaba, *Reac. Kin. Catal. Lett.* **2008**, *93*, 59.
[59] C. P. Hwang, C. T. Yeh, *J. Catal.* **1999**, *182*, 48.
[60] S. Damyanova, J. M. C. Bueno, *Appl. Catal. A: Gen.* **2003**, *253*, 135.
[61] D. González, E. Lima, N. Martin, *Ind. Eng. Chem. Res.* **2007**, *46*, 4335.
[62] L. V. Mattos, F. B. Noronha, *J. Power Sources* **2005**, *145*, 10.
[63] E. Rocchini, M. Vicario, J. Llorca, C. de Leitenburg, G. Dolcetti, A. Trovarelli, *J. Catal.* **2002**, *211*, 407.
[64] J. M. Gatica, R. T. Baker, P. Fornasiero, S. Bernal, J. Kaspar, *J. Phys. Chem. B* **2001**, *105*, 1191.
[65] R. S. Zhou, R. L. Snyder, *Acta Crystallogr., Sect. B: Struct. Sci.* **1991**, *47*, 617.
[66] G. Fagherazzi, P. Canton, P. Riello, F. Pinna, N. Pernicone, *Catal. Lett.* **2000**, *64*, 119.
[67] P. Riello, P. Canton, A. Benedetti, *Langmuir* **1998**, *14*, 6617.
[68] S. M. Kim, Y. J. Lee, J. W. Bae, H. S. Potdar, K. W. Jun, *Appl. Catal. A: Gen.* **2008**, *348*, 113.
[69] A. L. Alberton, M. M. V. M. Souza, M. Schmal, *Catal. Today* **2007**, *123*, 257.
[70] P. S. Gradeff, F. G. Schreiber, K. C. Brooks, R. E. Sievers, *Inorg. Chem.* **1985**, *24*, 1110.
[71] S. Enzo, S. Polizzi, A. Benedetti, *Z. Kristallogr.* **1985**, *170*, 275.
[72] P. Riello, P. Canton, G. Fagherazzi, *J. Appl. Crystallogr.* **1998**, *31*, 78.

Received: October 16, 2009
Revised: December 22, 2009
Published online on April 26, 2010

 © 2010 Wiley-VCH Verlag GmbH & Co. KGaA, Weinheim

1864564x, 2010, 5, Downloaded from https://chemistry-europe.onlinelibrary.wiley.com/doi/10.1002/cssc.200900243 by CONICET Consejo Nacional de Investigaciones, Wiley Online Library on [07/12/2023]. See the Terms and Conditions (https://onlinelibrary.wiley.com/terms-and-conditions) on Wiley Online Library for rules of use; OA articles are governed by the applicable Creative Commons License